Pressure evolution of electrical transport in the 3D topological insulator $(Bi,Sb)_2(Se,Te)_3$

2015 J. Phys.: Conf. Ser. 592 012124

(http://iopscience.iop.org/1742-6596/592/1/012124)

Journal of Physics: Conference Series **592** (2015) 012124 doi:10.1088/1742-6596/592/1/012124

Pressure evolution of electrical transport in the 3D topological insulator $(Bi,Sb)_2(Se,Te)_3$

J R Jeffries,[1] N P Butch,[1,2] Y K Vohra,[3] and S T Weir[1]

[1] Condensed Matter and Materials Division, Lawrence Livermore National Laboratory, Livermore, California 94550, USA
[2] NIST Center for Neutron Research, National Institute of Standards and Technology, Gaithersburg, MD, 20899 USA
[3] Department of Physics, University of Alabama at Birmingham, Birmingham, Alabama 35294, USA

E-mail: jeffries4@llnl.gov

Abstract. The group V-VI compounds—like Bi_2Se_3, Sb_2Te_3, or Bi_2Te_3—have been widely studied in recent years for their bulk topological properties. The high-Z members of this series form with the same crystal structure, and are therefore amenable to isostructural substitution studies. It is possible to tune the Bi-Sb and Te-Se ratios such that the material exhibits insulating behavior, thus providing an excellent platform for understanding how a topological insulator evolves with applied pressure. We report our observations of the pressure-dependent electrical transport and crystal structure of a pseudobinary $(Bi,Sb)_2(Te,Se)_3$ compound. Similar to some of its sister compounds, the $(Bi,Sb)_2(Te,Se)_3$ pseudobinary compound undergoes multiple, pressure-induced phase transformations that result in metallization, the onset of a close-packed crystal structure, and the development of distinct superconducting phases.

Since the demonstration of the presence of Dirac cones and chiral surface states in the 3D topological insulators Bi_2Te_3 and Bi_2Se_3 [1, 2], substantial work on "band-structure engineering" of the group V-VI chalcogenides has been undertaken in an effort to disentangle this surface state from the bulk carriers. Differing routes to this goal have been attempted, including optimized synthesis [3], chemical substitution [4, 5, 6], and the application of high pressures [7, 8, 9, 10, 11, 12, 13, 14]. Interestingly, some of these experiments have shown a proclivity for superconductivity, either with sufficient doping or pressure [4, 9, 10, 11, 14, 15], providing tantalizing prospects for quantum computation or spintronic applications.

While the superconducting states of Bi_2Te_3, Bi_4Te_3, Bi_2Se_3, and Sb_2Te_3 can be induced with pressure, the crystal structure is also susceptible to a series of pressure-induced phase transformations. In general, these compounds realize a high-symmetry crystal structure (shown to be body-centered-cubic for all except Bi_2Se_3) at the highest pressures [7, 9, 15], and this phase supports the highest superconducting critical temperature T_c. With pressure, Bi_2Te_3 can support superconductivity within the ambient-pressure crystal structure [11], raising an interesting question as to the roles of crystal structure and band structure in manifesting superconductivity.

To address the potential competition between band and crystal structures, we have synthesized a pseudo-binary alloy of $(Bi,Sb)_2(Se,Te)_3$ that displays insulating characteristics in electrical transport at ambient pressure. Under pressure, this compound undergoes a series of

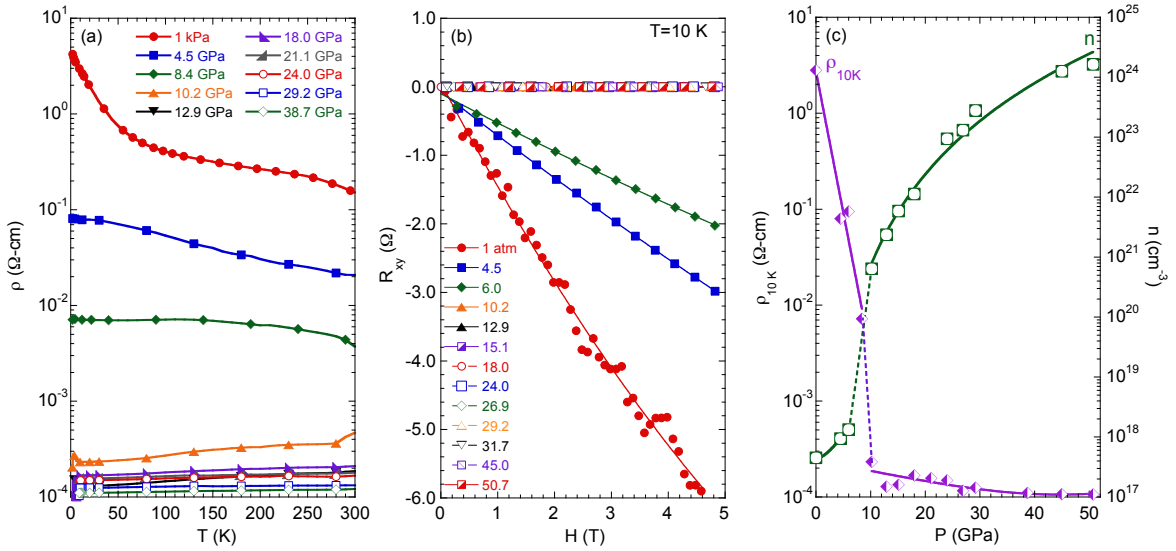

Figure 1. (color online) (a) Temperature-dependent electrical resistivity $\rho(T)$ for a sample of BSTS at selected pressures, showing the loss of insulating behavior and the development of metallic conduction near 10.2 GPa (logarithmic vertical axis). (b) Transverse magnetoresistance R_{xy} versus magnetic field at 10 K for selected pressures. The slope of $R_{xy}(H)$ decreases with increasing pressure, showing characteristic metallic behavior at pressures above 10.2 GPa. (c) The value of ρ at 10 K and the carrier concentration, determined from (b), as functions of pressure; a clear transition is visible in both quantities at 10.2 GPa. Pressures in the legends of (a) and (b) are given in GPa, where not specified. In each panel, lines are guides to the eye.

structural phase transformations, concomitantly metallizing with the first phase transformation. The high-pressure, metallic phases support two superconducting states, the appearance of which are tied to changes in crystal structure. These results are very similar to those obtained for the other compounds in this family, indicating that superconductivity is dictated by the crystal structure more than the initial electronic structure.

Samples were grown from a stoichiometric melt using the following constituent materials: 99.999% Bi (ESPI Metals), 99.99% Sb (ESPI Metals), 99.999% Se (ESPI Metals), and 99.999% Te (ESPI Metals). The stoichiometry of the pseudo-binary alloy was $(Bi_{0.75}Sb_{0.25})_2(Se_{0.43}Te_{0.57})_3$ (*i.e.*, $Bi_{1.5}Sb_{0.5}Se_{1.3}Te_{1.7}$); hereafter, for brevity, this stoichiometry will be referred to as BSTS. The constituent elements were loaded into an alumina crucible, and sealed in a quartz tube under a partial pressure of ultra-high purity argon. The quartz tube was heated in a box furnace to 850 °C and held for 48 hours, after which the system was allowed to cool to 550 °C over the course of 100 hours. The tube was removed from the furnace, and the samples were extracted from the alumina crucible. Large, single-crystal plates ($\approx$1 cm^2 in area) were cleaved from the solid mass. The crystal structure was confirmed to be single phase by x-ray diffraction, and a Laue backscatter image revealed the single-crystal nature of the samples.

Electrical transport under pressure was measured using a screw-driven, BeCu diamond anvil cell (DAC) that employed one blank 300-μm diamond anvil paired with a 270-μm designer diamond anvil [16]. Tungsten electrical contact pads were sputtered onto the microprobes on the culet of the designer diamond to facilitate electrical contact. A small piece ($\approx$ 50 x 50 μm) of sample was loaded into the sample chamber in direct contact with the microprobes. An MP35N gasket was used in conjunction with steatite as the pressure-transmitting medium.

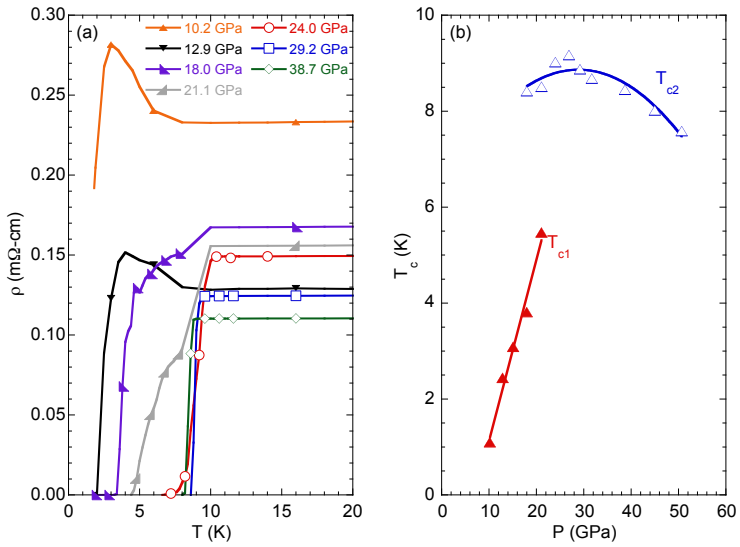

Figure 2. (color online) (a) Example, low-temperature electrical resistivity $\rho(T)$ for a sample of BSTS at selected pressures, revealing the development of superconductivity above 10.2 GPa (linear vertical axis). (b) The pressure-dependent evolution of T_c; two superconducting phases are evidenced by the pressure dependence and the coexistence of two transitions between 18 and 21 GPa. Pressures in the legend of (a) are given in GPa, where not specified. Lines are guides to the eye.

Temperature- and field-dependent measurements were performed in a Quantum Design Physical Property Measurement System.

In addition, room-temperature x-ray diffraction experiments were performed at Sector 16 BM-D (HPCAT) of the Advanced Photon Source. These experiments employed a membrane-driven diamond anvil cell composed of 300-μm diamond anvils. A powdered sample was loaded into a rhenium gasket, and neon was used as a pressure-transmitting medium. A 30-keV x-ray beam was focused to a size of 5 x 12 μm, and diffraction was collected in a transmission geometry using an image plate. 2D diffraction patterns were collapsed to conventional 1D intensity versus 2Θ patterns using the program FIT2D [17].

Figure 1a reveals the pressure and temperature dependence of the electrical resistivity, $\rho(T)$ of BSTS. At ambient pressure, BSTS shows insulating behavior with a resistance that decreases with increasing temperature. With pressure, this behavior becomes less pronounced, and above 10.2 GPa, the temperature dependence of ρ exhibits a linear temperature dependence, suggestive of the development of a metallic state. Magnetotransport measurements at 10 K further confirm the metallic nature of the high-pressure state of BSTS. Figure 1b shows the anti-symmetrized, transverse magnetoresistance, R_{xy}, versus magnetic field. At low pressure, the slope is large, indicative of a small carrier density and consistent with the insulating character observed in the $\rho(T)$ measurements at low pressure. However, above 10.2 GPa, the transverse magnetoresistance becomes small and maintains a low slope up to the highest pressures measured, indicative of metallic conduction. The value of ρ(10 K) and the carrier density extracted from the transverse magnetoresistance are plotted in Fig. 1c. There is a clear transition in the pressure-dependence of the carrier density near 10.2 GPa; and ρ(10 K) mirrors the carrier density, showing a similar discontinuity at 10.2 GPa.

As shown in Fig. 2, at low temperatures, the pressure-induced metallic state shows

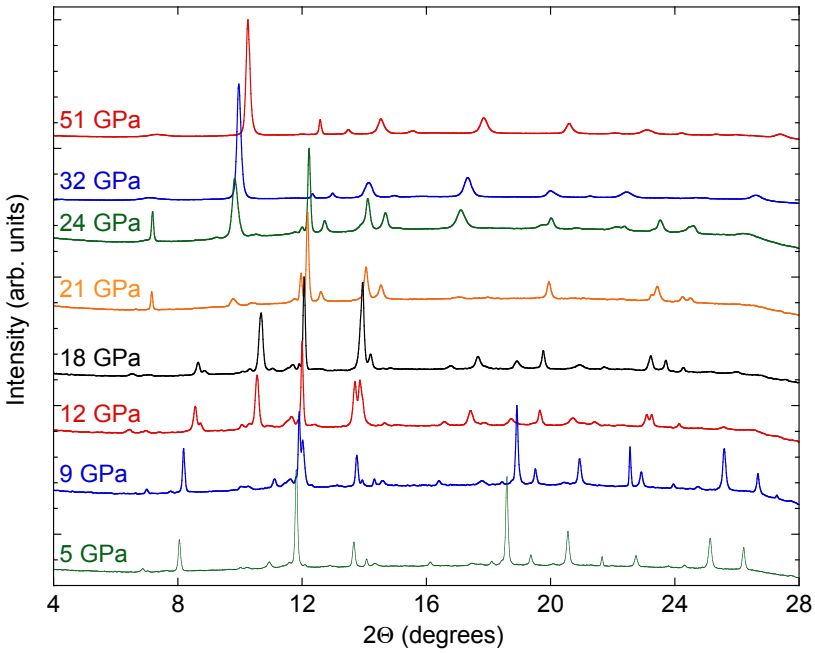

Figure 3. (color online) Selected x-ray diffraction patterns showing the signatures of structural phase transitions under pressure. The main peaks of the highest pressure structures are consistent with a body-centered-cubic phase.

superconductivity near T_c=2.4 K at P =12.9 GPa. With pressure, T_c increases linearly up to a value of T_c=5.5 K at P =21.1 GPa. At 18.0 GPa, two transitions become evident in the $\rho(T)$ curve. The lower T_c appears to yield to the higher temperature transition, leaving only a single superconducting transition above 21.1 GPa. This higher temperature transition peaks at T_c=9.2 K at 26.8 GPa. Further pressure drives T_c down, but T_c remains above 7.5 K at the highest pressure measured, 50.7 GPa.

Room-temperature x-ray diffraction results clearly show changes in the diffraction patterns, and thus crystal structures, under pressure. Between 9 and 12 GPa, the ambient-pressure structure transforms to a high-pressure phase (Phase-II), which seems to persist up to 21 GPa. At 21 GPa another phase transition occurs into phase Phase-III, as evidenced by the appearance of the diffraction peak near 7.2 degrees. Finally, at the highest pressures, a body-centered-cubic (bcc) phase is realized (Phase-IV). It should be noted that the bcc phase extends down in pressure to at least 24 GPa, meaning that the phase field for Phase-III is fairly small. Because of the widths of the phase fields, the superconducting states shown in Fig. 2b are most likely associated with Phase-II (low-temperature T_c) and Phase-IV (high-temperature T_c). Though the intervening structures, Phases-II and -III, have not been determined, the overall structural evolution with pressure is very similar to the sister compounds Bi_2Te_3, Bi_4Te_3, and Bi_2Se_3, albeit with slightly different transformation pressures.

In summary, despite substantially different ambient-pressure electrical transport with respect to its siblings, BSTS behaves very similar to that of other V-VI chalcogenides under pressure. The application of pressure results in phase transformations to crystal structures that exhibit metallic behavior and support superconductivity. No dramatic differences in this general high-

pressure behavior were observed due to the more insulating nature of BSTS.

Acknowledgments
This work was performed under LDRD (14-ERD-041). Lawrence Livermore National Laboratory is operated by Lawrence Livermore National Security, LLC, for the U.S. Department of Energy, National Nuclear Security Administration under Contract DE-AC52-07NA27344. Portions of this work were performed at HPCAT (Sector 16), Advanced Photon Source (APS), Argonne National Laboratory. HPCAT operations are supported by DOE-NNSA under Award No. DE-NA0001974 and DOE-BES under Award No. DE-FG02-99ER45775, with partial instrumentation funding by NSF. APS is supported by DOE-BES, under Contract No. DE-AC02-06CH11357. YKV acknowledges support from DOE-NNSA Grant No. DE-FG52-10NA29660. Identification of commercial materials or equipment does not imply recommendation or endorsement by the National Institute of Standards and Technology, nor does it imply that the materials or equipment identified are necessarily the best available for the purpose.

References
[1] Chen Y L, *et al.*, 2009 *Science* **325**, 178.
[2] Xia Y, *et al.*, 2009 *Nat. Phys.* **5**, 398.
[3] Butch N P, Kirshenbaum K, Syers P, Sushkov A B, Jenkins G S, Drew H D, and Paglione J, 2010 *Phys. Rev. B* **81**, 241301(R).
[4] Hor Y S, Williams A J, Checkelsky J G, Roushan P, Seo J, Xu Q, Zandbergen H W, Yazdani A, Ong N P, and Cava R J, 2010 *Phys. Rev. Lett.* **104**, 057001.
[5] Ren Z, Taskin A A, Sasaki S, Segawa K, and Ando Y, 2011 *Phys. Rev. B* **84**, 165311.
[6] Arkane T, Sato T, Souma S, Kosaka K, Nakayama K, Komatsu M, Takahashi T, Ren Z, Segawa K, and Ando Y, 2012 *Nat. Comm.* **3**, 636.
[7] Nakayama A, Einaga M, Tanabe Y, Nakano S, Ishikawa F, and Yamada Y, 2009 *J. High Press. Res.* **29**, 245.
[8] Zhao J, Liu H, Ehm L, Chen Z, Sinogeiken S, Zhao Y, and Gu G, 2011 *Inorg. Chem.* **50**, 11291.
[9] Jeffries J R, Lima Sharma A L, Sharma P A, Spataru C D, McCall S K, Sugar J D, Weir S T, and Vohra Y K, 2011 *Phys. Rev. B* **84**, 092505.
[10] Zhang J L, *et al.*, 2011 *Proc. Natl. Acad. Sci.* **108**, 24.
[11] Zhang C, Sun L, Chen Z, Zhou X, Wu Q, Yi W, Guo J, Dong X, and Zhao Z, 2011 *Phys. Rev. B* **83**, 140504(R).
[12] Vilaplana R, *et al.*, 2011 *Phys. Rev. B* **84**, 184110.
[13] Hamlin J J, Jeffries J R, Butch N P, Syers P, Zocco D A, Weir S T, Vohra Y K, Paglione J, and Maple M B, 2012 *J. Phys. Condens. Matt.* **24**, 035602.
[14] Kirshenbaum K, Syers P S, Hope A P, Butch N P, Jeffries J R, Weir S T, Hamlin J J, Maple M B, Vohra Y K, and Paglione J, 2013 *Phys. Rev. Lett.* **111**, 087001.
[15] Zhu J, *et al.*, 2013 *Sci. Rep.* **3**, 2016.
[16] Jeffries J R, Butch N P, Kirshenbaum K, Saha S R, Samudrala G, Weir S T, Vohra Y K, and Paglione J, 2012 *Phys. Rev. B* **85**, 18450.
[17] Hammersley A, Svensson S, Hanfland M, Fitch A, and Häusermann D, 1996 *High Press. Res.* **14**, 235.